Applied Surface Science 387 (2016) 103–108

Contents lists available at ScienceDirect

Applied Surface Science

journal homepage: www.elsevier.com/locate/apsusc

Enhanced field emission from ZnO nanowire arrays utilizing MgO buffer between seed layer and silicon substrate

Si Chen [a], Jiangtao Chen [b], Jianlin Liu [c], Jing Qi [a,*], Yuhua Wang [d,*]

[a] The Key Laboratory for Magnetism and Magnetic Materials of MOE, School of Physical Science and Technology, Lanzhou University, Lanzhou 730000, China
[b] State Key Laboratory of Solid Lubrication, Lanzhou Institute of Chemical Physics, Chinese Academy of Sciences, 18 Tianshui Mid. Road, Lanzhou 730000, China
[c] Quantum Structures Laboratory, Department of Electrical and Computer Engineering, University of California, Riverside, CA 92521, USA
[d] Department of Material Science, School of Physical Science and Technology, Lanzhou University, Lanzhou 730000, China

ARTICLE INFO

Article history:
Received 25 March 2016
Received in revised form 13 June 2016
Accepted 15 June 2016
Available online 17 June 2016

Keywords:
ZnO nanowire arrays
Field emission
MgO buffer layer
Electron transport
Vertically aligned

ABSTRACT

Field emitters based on ZnO nanowires and other nanomaterials are promising high-brightness electron sources for field emission display, microscopy and other applications. The performance of a ZnO nanowire field emitter is linked to the quality, conductivity and alignment of the nanowires on a substrate, therefore requiring ways to improve these parameters. Here, ZnO nanowire arrays were grown on ZnO seed layer on silicon substrate with MgO buffer between the seed layer and Si. The turn-on field and enhancement factor of these nanowire arrays are 3.79 V/μm and 3754, respectively. These properties are improved greatly compared to those of ZnO nanowire arrays grown on ZnO seed layer without MgO buffer, which are 5.06 V/μm and 1697, respectively. The enhanced field emission properties can be attributed to better electron transport in seed layer, and better nanowire alignment because of MgO buffer.

1. Introduction

Zinc oxide (ZnO) has attracted a great deal of attention in recent years as a wide band gap (3.37 eV) semiconducting, piezoelectric, and photoconducting material [1–3]. It is promising for exciton-based applications because of its high exciton binding energy of 60 meV. ZnO nanostructures have also been studied extensively for their great potential in applications in optoelectronic devices [4], field effect transistors [5], waveguides [6], photocatalysis [7], sensors [8], surface acoustic solar cells [9], and field emitters [10]. Among various ZnO nanostructures, vertical one-dimensional (1D) ZnO nanostructures such as nanowire, nanorod and nanotip arrays are expected to act as functional building blocks for future electronics including nanogenerator, field emitter and other nanoscale systems [11]. Take nanogenerator as an example, growth of orientation-, position-, and size-controlled nanowire arrays is the key for raising the output voltage and power [12]. Meanwhile, the alignment is an important factor for field emission (FE) properties [13]. All kinds of fabrication methods such as vapor transfer process [14], metal organic chemical vapor deposition [15], thermal evaporation [16] and hydrothermal synthesis [17] have been utilized to prepare 1D ZnO nanostructures.

Silicon and sapphire wafers are widely utilized as substrates to fabricate ZnO based devices. Compared with sapphire wafers, silicon wafers have advantages such as lower cost and resistivity. ZnO nanowire arrays on Si wafer have not reached satisfactory quality because of the large stress as well as their chemical dissimilarities [18,19]. Metal catalysts such as Au have been used to assist and control ZnO growth on Si substrates [20]. However, after this vapor-liquid-solid (VLS) process, the residual catalysts may be a source of contamination that will influence the purity of ZnO nanowire arrays. On the other hand, the vapor-solid (VS) route appears to be more versatile because it is not confined by the catalyst nanoparticles. It was reported that a thin film of ZnO seed layer was utilized as the nucleation template to grow well aligned high-quality ZnO nanowires by vs methods [21]. However, there is still a large strain at the interface of the ZnO seed layer and Si substrate due to their large lattice mismatch. The lattice mismatch could have a detrimental impact on the crystallinity of ZnO seed layer, which degrades the electron transport, and in turn, affects the FE properties of field emitters and electrical properties of other ZnO based devices such as solar cells, photodetectors and light emitting diodes [3]. Epitaxial synthesis of 1D ZnO nanowire arrays on ZnO substrates would provide a high-quality interface, which is favorable for electrical

* Corresponding authors.
E-mail addresses: qijing@lzu.edu.cn (J. Qi), wyh@lzu.edu.cn (Y. Wang).

http://dx.doi.org/10.1016/j.apsusc.2016.06.085
0169-4332/

properties. However, single-crystal ZnO wafers are not cost effective for the moment.

Meanwhile, buffer layers including amorphous and crystalline ones are widely used in the field of 2D heteroepitaxial film growth on various substrates to improve the active film quality [22,23]. One of the popular buffer layers for ZnO epitaxy is MgO [22–24]. MgO is thermodynamically stable, and also has low dielectric constant. Both lattice mismatches between MgO and ZnO and between MgO and silicon are lower than that between ZnO and silicon [25]. High-quality ZnO thin films have been grown on Si (100) substrates by utilizing MgO as buffer layers [25,26]. However, the effect of MgO buffer layer between the ZnO seed layer and Si substrate on the growth of ZnO nanowire arrays on top and the FE properties of the nanowire arrays has not been reported yet. In this paper, we report better field emission properties from ZnO nanowire arrays grown on ZnO seed layer on Si with a MgO layer as the buffer than that without MgO buffer. The reasons of the improvement of FE properties are discussed.

2. Experimental details

2.1. Synthesis of ZnO nanowire arrays

ZnO nanowire arrays were synthesized by chemical vapor deposition (CVD) on ZnO thin film seed layers. ZnO seed layers with and without MgO buffer were grown on pre-cleaned p^+-Si (100) substrates in a radio frequency plasma-assisted SVTA molecular beam epitaxy system [27]. Zn and Mg sources were provided by regular Knudsen-cells filled with elemental Zn (6N) and Mg (6N), respectively. O source was provided by a radio frequency plasma source sustained with O_2 (6N) gas. A mass flow controller was used to precisely tune the O_2 flow rate. MgO thin film was grown on Si substrate at 350 °C with 455 °C Mg cell temperature, 5.0 sccm (standard cubic centimeter per minute) O_2 gas flow rate, and 400 W oxygen plasma power, followed by a ZnO buffer layer growth at 350 °C, for 1 min to improve subsequent ZnO seed layer quality. The ZnO layers were grown on MgO buffer layer or directly on Si substrate at 550 °C, with Zn cell temperature of 345 °C, O_2 gas flow rate of 5.0 sccm, and oxygen plasma power of 400 W. The thickness of the seed layers is around 140 nm. Then the two ZnO seed layer substrates with and without MgO buffer were transferred to a CVD quartz tube furnace. Analytical grade zinc powder (purity 99.99%) was employed as Zn source. The source material was placed in a quartz boat located in the center of the tube. The substrates were placed downstream of the carrier gas flow. The quartz tube was purged with 500 sccm of argon and 0.8 sccm of oxygen during the entire furnace process of nanowire growth. The pumping speed of a mechanical pump was regulated to maintain the pressure inside the quartz tube at the lowest level during the evaporation. Then the furnace temperature was raised to 700 °C at a rate of 10 °C/min. After growth for 30 min, the furnace was cooled naturally down to room temperature.

2.2. Characterizations and measurements of the obtained nanoarrays

The crystal structure and chemical nature of ZnO nanowire arrays were analyzed using X-ray diffractometry (XRD) (parallel lights) with Cu K-alpha radiation (=1.54187 Å) operating at 40 kV and 20 mA. The morphology of the samples was obtained utilizing a field emission scanning electron microscope (FESEM). The interface is characterized by atomic resolution scanning transmission electron microscopy (STEM) and the elemental map is characterized by STEM electron energy loss spectroscopy (EELS). The FE properties were measured in vacuum at a pressure of 5×10^{-6} Pa, a distance of 300 μm, and a temperature of about 300 K.

3. Results and discussion

3.1. Crystallinity and surface morphology

Fig. 1(a) and (b) show SEM images of the surface morphology of ZnO seed layers with and without MgO buffer, respectively. The scale bars are 200 nm. The grains of ZnO seed layer with MgO buffer are more regular than that without MgO buffer. When nanowire arrays are grown on ZnO seed layer with MgO buffer (denoted as nanowire arrays with MgO buffer), they are relatively more vertically aligned than those grown on ZnO seed layer without MgO buffer layer (denoted as nanowire arrays without MgO layer), as shown in the top-view (Fig. 1(c) for nanowire arrays with MgO layer and Fig. 1(d) for nanowire arrays without MgO layer) and side-view (Fig. 1(e) for nanowire arrays with MgO layer and Fig. 1(f) for nanowire arrays without MgO layer) SEM images, respectively. The inset of Fig. 1(c) shows a high-magnification image of a single nanowire, indicating that the nanowires are c-oriented. The scale bars are 500 nm. The diameter and length of the nanowires are about 35 nm, 4.3 μm, respectively.

Fig. 2 shows XRD patterns of the two ZnO nanowire array samples. Both nanowire arrays exhibit the preferred orientation of (001), which is consistent with the theory that ZnO is usually grown with c-axis preferred orientation under typical growth conditions because of the lowest surface energy of the (001) basal plane in ZnO [28]. The degree of the orientation can be illustrated by the relative texture coefficient [29], which is given by

$$TC_{002} = \frac{I_{002}/I^0_{002}}{I_{002}/I^0_{002} + I_{103}/I^0_{103}}$$

where TC_{002} is the relative texture coefficient of diffraction peaks (002) over (103), I_{002} and I_{103} are the measured diffraction peak intensities due to (002) and (103) planes, respectively, $I^0{}_{002}$ and $I^0{}_{103}$ are the corresponding values of standard PDF card measured from randomly oriented powder samples. For materials with random crystallographic orientations, e.g. powders, the texture coefficient is 0.5. For nanowire arrays with MgO layer, the calculated TC_{002} is 1, which means the nanowire arrays with MgO layer are totally c-oriented. The lattice constant is c = 5.205 Å. For nanowire arrays without MgO layer, the calculated TC_{002} is 0.756, which means the directions of the nanowires are relatively diverse. The lattice parameters are a = 3.252 Å, c = 5.205 Å. Both patterns are in good agreement with the standard values (JCPDS card No. 36-1451: a = 3.2498 Å c = 5.2066 Å). These results reveal that the synthesized ZnO nanowires have good crystalline wurtzite structure.

3.2. Characterizations of substrates

The STEM annular bright field (ABF) and the elemental map of the selected area by STEM EELS spectrum images for the interface of LT-ZnO/MgO/Si are shown in Fig. 3. Fig. 3(a) is the STEM annular bright field image. Fig. 3(b)–(e) are elemental maps of (b) O, (c) Zn, (d) Mg, and (e) Si. Fig. 3 shows that the middle layer between Si substrate and LT-ZnO layer is amorphous MgO.

Since crystal quality of ZnO seed layer can affect the electron transport, and in turn, FE properties [3], XRD was utilized to estimate effect of amorphous MgO layer on the crystal quality of the seed layers. As can be seen from the XRD spectra in Fig. 4, both ZnO seed layers have wurtzite crystalline structure. For ZnO seed layer with MgO buffer, only (002) peak appears, indicating that it is highly c-oriented. Meanwhile, XRD pattern of ZnO seed layer without MgO buffer shows multiple peaks, indicating that it is lowly c-oriented. The lattice constants of ZnO seed layers with and without MgO buffer are c = 5.2093 Å, and a = 3.2543 Å, c = 5.2123 Å, respectively,

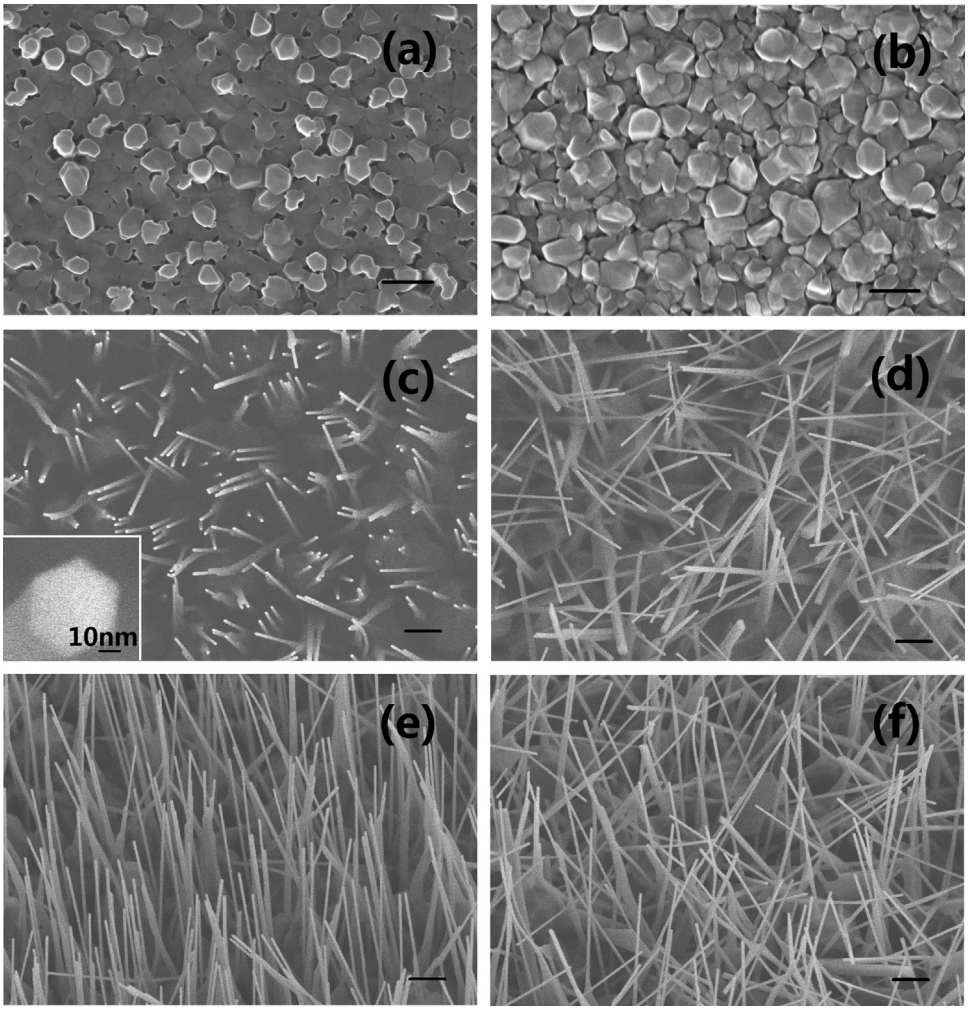

Fig. 1. SEM images of surface morphologies of ZnO seed layers (a) with and (b) without MgO buffer. The scale bars are 200 nm. The grains of ZnO seed layer with MgO buffer are more regular than that without MgO buffer. (c) and (d) are top view SEM images of nanowire arrays with MgO layer and nanowire arrays without MgO layer, respectively. (e) and (f) are side view SEM images of nanowire arrays with MgO layer and nanowire arrays without MgO layer, respectively. The scale bars are 500 nm. The inset of (c) shows high-magnification SEM image of a single nanowire. Nanowire arrays with MgO layer are more vertically aligned than those without MgO layer.

which are in good agreement with the standard values (JCPDS card No. 36-1451: a = 3.2498 Å c = 5.2066 Å). The full-width at half maximum (FWHM) of the (002) peak for ZnO seed layers with and without MgO buffer are 0.351 and 0.447, respectively. The smaller FWHM value of the XRD peak for ZnO seed layer with MgO buffer implies better crystallinity, which could benefit electron transport. It is also evident that there is a correlation between the morphology of the ZnO nanowires and surface orientation of the seed layer. Highly c-oriented seed layer as a result of MgO buffer results in nanowire arrays with good alignment and high c-orientation, while lowly c-oriented seed layer without MgO buffer leads to severely titled alignment of the nanowires [30], as shown in Fig. 1.

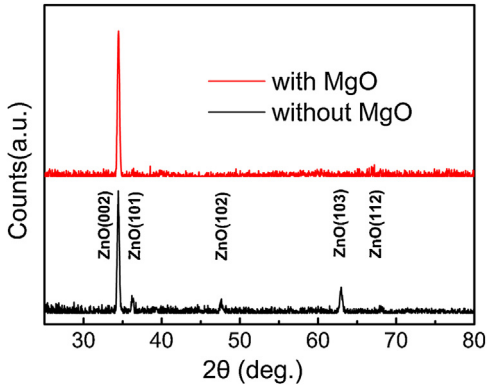

Fig. 2. XRD patterns of nanowire arrays with and without MgO layer. Both arrays show c-axis preferred orientation. Nanowire arrays with MgO layer are more highly c-oriented than those without MgO layer.

The residual stress σ in the ZnO seed layers can be obtained using [31]

$$\sigma_{film} = -232.81GPa \times \frac{c_{film} - c_{bulk}}{c_{bulk}}$$

where c_{bulk} is lattice constant of bulk ZnO, which is 5.206 Å, c_{film} is lattice constant of the film calculated from XRD patterns. For ZnO seed layer with and without MgO buffer, σ_{film} are −0.12 GPa and −0.25 GPa, respectively. The larger difference between lattice constants of the film and bulk ZnO leads to higher residual stress. ZnO seed layer without MgO buffer has higher residual stress, which could lead to lower crystallinity [18], and in turn, degraded FE properties [3].

To characterize the electron transport of two substrates, we measured the resistances from top to bottom (noted as top-bottom resistance) of the two kinds of substrates. The top-bottom resistances of 1 cm × 1 cm pieces of ZnO seed layer with and without

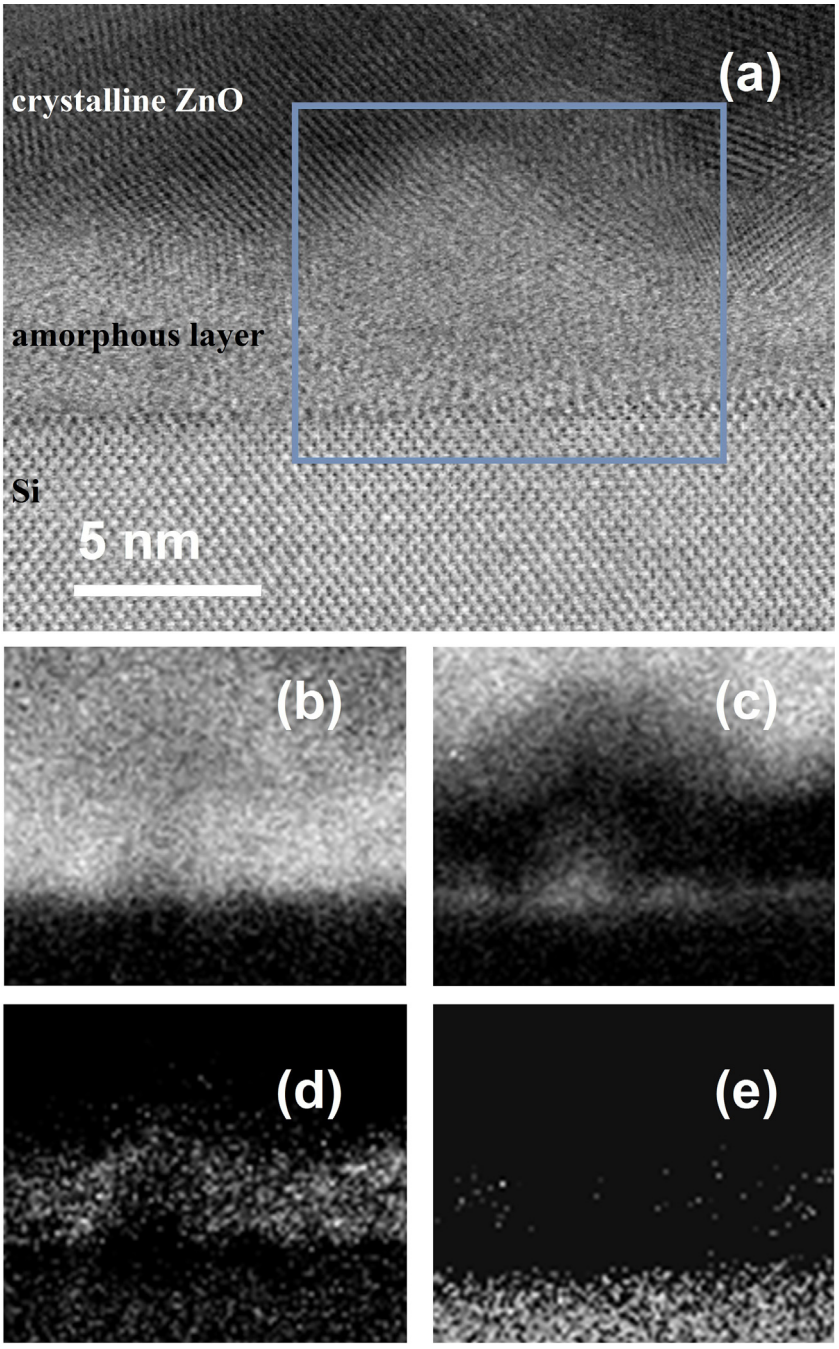

Fig. 3. STEM ABF image (a) of LT-ZnO/MgO/Si interface and elemental maps of the selected square area in (a) for (b) O, (c) Zn, (d) Mg, and (e) Si. STEM ABF images and Elemental maps show that the middle layer is amorphous MgO layer.

MgO buffer are about 100 Ω and 5 KΩ, respectively. MgO is a wide band gap semiconductor. Insertion of such material (about 5 nm) could hamper the overall electron transport. However, insertion of MgO buffer could also lead to a better crystallinity of the LT-ZnO layer, which is of benefit to electron transport. Obviously, the latter has a greater impact on the electron transport.

3.3. FE properties

Fig. 5 shows FE properties of nanowire arrays with and without MgO layer. The turn-on electric field value, which is defined as the average field between the anode and cathode as the emission current density reaches 0.1 mA/cm^2 [32], is about 3.79 V/μm for nanowire arrays with MgO layer. The Fowler-Nordheim (FN) plots in the inset of Fig. 5 shows a roughly linear relationship for nanowire arrays with MgO layer, implying that a quantum tunneling mechanism is responsible for the emission [33]. For the FN emission,

$$J = \left(A\beta^2 E^2/\varphi\right) exp\left(-B\varphi^{\frac{2}{3}}/\beta E\right)$$

where J is current density, E is applied field strength, φ is work function of the emitter material (5.3 eV for ZnO), A and B are constant with a value of 1.56×10^{-10} (AV^{-2} eV) and 6.83×10^3 (VeV$^{-3/2}$ μm^{-1}), respectively, and β is field enhancement factor, which is associated with the magnitude of electric field at the emitting surface by $E_{local} = \beta E$, E_{local} is the local electric field at the

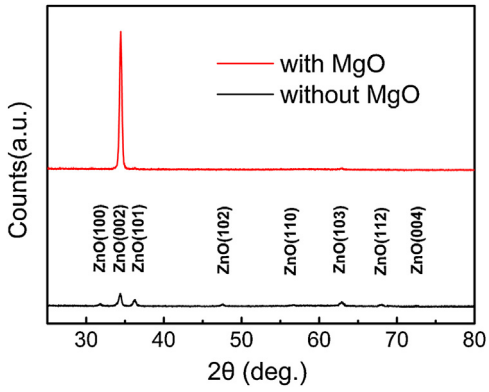

Fig. 4. XRD pattern of ZnO seed layers with and without MgO buffer. ZnO seed layer with MgO buffer has higher crystallinity and better preferred orientation of (002).

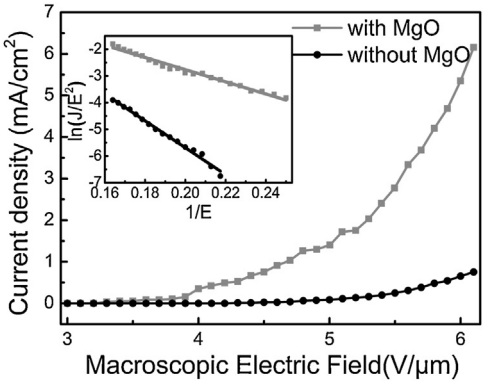

Fig. 5. *J*/*E* plots of the two nanowire array samples. The inset shows corresponding FN plots, the FN plots can be simulated as straight lines, implying FN emissions. Nanowire arrays with MgO buffer layer show better FE properties of low turn-on field and high field enhancement factor.

emitting surface. Based on the slope from plotting $\ln(J/E^2)$ versus $1/E$ in the inset of Fig. 5, β is estimated to be approximately 3754 for nanowire arrays with MgO layer. Such a high enhancement factor could enable various field emission applications. As a comparison, nanowire arrays without MgO layer exhibit a lower enhancement factor of 1697 and higher turn-on field of 5.06 V/μm. The results confirm that FE properties of nanowire arrays grown on ZnO seed layer by utilizing MgO as buffer layer are superior to the nanowire arrays grown on ZnO seed layer without MgO buffer layer. As shown in Fig. 1, the nanowire arrays with MgO are more vertically aligned. It has been found that better alignment could lead to better FE properties. This is believed to be due to the screening effect of ZnO nanowire arrays without MgO buffer, which are entangled together on the surface where the arrays of electron emitting nanowires tips are not aligned regularly [34]. Such phenomenon has also been reported in other systems [35,36]. As shown in Section 3.2, the electron transport of ZnO seed layer with MgO buffer is better than that without buffer. The improvements of both alignment and electron transport result in better FE properties.

4. Conclusion

In summary, ZnO nanowires were synthesized by CVD at 700 °C using a thin ZnO film as seed layer through vs mechanism. Two kinds of ZnO seed layers grown on silicon were utilized as substrates to prepare ZnO nanowire arrays. One kind of substrates utilizes amorphous MgO thin film as buffer between ZnO seed layer and Si substrate. The other is ZnO seed layer epitaxially grown on Si substrate directly. With MgO buffer, the ZnO seed layer shows lower top-bottom resistance than that without MgO buffer. The nanowire arrays grown on ZnO seed layer with MgO buffer show low turn-on field and high enhancement factor, which indicate better FE properties when compared to nanowire arrays grown on seed layer without MgO buffer. The better FE properties of nanowire arrays with MgO layer could attribute to better electron transport and nanowire alignment. Our work offers a potential method to enhance the performance of ZnO based field-emission devices.

Acknowledgements

This work was supported by National Natural Science Foundation of China (No. 50902065, 11474137, 51402139), Open Project of Key Laboratory for Magnetism and Magnetic Materials of the Ministry of Education, Lanzhou University (LZUMMM2015012), National Nature Science Young Foundation of China (no. 10904057).

References

[1] R. Chen, Q. Ye, T. He, V.D. Ta, Y. Ying, Y.Y. Tay, T. Wu, Exciton localization and optical properties improvement in nanocrystal-embedded ZnO core–shell nanowires, Nano Lett. 13 (2013) 734–739.
[2] S.A. Kulinich, T. Kondo, Y. Shimizu, T. Ito, Pressure effect on ZnO nanoparticles prepared via laser ablation in water, J. Appl. Phys. 113 (2013) 33509.
[3] J. Song, S.A. Kulinich, J. Yan, Z. Li, J. He, C. Kan, H. Zeng, Epitaxial ZnO nanowire-on-nanoplate structures as efficient and transferable field emitters, Adv. Mater. 25 (2013) 5750–5755.
[4] S. Chu, G. Wang, W. Zhou, Y. Lin, L. Chernyak, J. Zhao, J. Kong, L. Li, J. Ren, J. Liu, Electrically pumped waveguide lasing from ZnO nanowires, Nat. Nanotechnol. 6 (2011) 506–510.
[5] R. Ahmad, N. Tripathy, Y. Hahn, Highly sensitive hydrazine chemical sensor based on ZnO nanorods field-effect transistor, Chem. Commun. 50 (2014) 1890–1893.
[6] I. Yoon, S.E. Baker, K. Kim, Y. Wang, S.C. Esener, D.J. Sirbuly, Profiling the evanescent field of nanofiber waveguides using self-assembled polymer coatings, Nanoscale 5 (2013) 552–555.
[7] X. Bai, L. Wang, R. Zong, Y. Lv, Y. Sun, Y. Zhu, Performance enhancement of ZnO photocatalyst via synergic effect of surface oxygen defect and graphene hybridization, Langmuir 29 (2013) 3097–3105.
[8] D. Gedamu, I. Paulowicz, S. Kaps, O. Lupan, S. Wille, G. Haidarschin, Y.K. Mishra, R. Adelung, Rapid fabrication technique for interpenetrated ZnO nanotetrapod networks for fast UV sensors, Adv. Mater. 26 (2014) 1541–1550.
[9] S.H. Ko, D. Lee, H.W. Kang, K.H. Nam, J.Y. Yeo, S.J. Hong, C.P. Grigoropoulos, H.J. Sung, Nanoforest of hydrothermally grown hierarchical ZnO nanowires for a high efficiency dye-sensitized solar cell, Nano Lett. 11 (2011) 666–671.
[10] M. Deo, D. Shinde, A. Yengantiwar, J. Jog, B. Hannoyer, X. Sauvage, M. More, S. Ogale, Cu2O/ZnO hetero-nanobrush: hierarchical assembly, field emission and photocatalytic properties, J. Mater. Chem. 22 (2012) 17055–17062.
[11] G. Yi, C. Wang, W.I. Park, ZnO nanorods: synthesis, characterization and applications, Semicond Sci. Tech. 20 (2005) S22.
[12] J. Liu, P. Fei, J. Zhou, R. Tummala, Z.L. Wang, Toward high output-power nanogenerator, Appl. Phys. Lett. 92 (2008) 173105.
[13] J.O. Hwang, D.H. Lee, J.Y. Kim, T.H. Han, B.H. Kim, M. Park, K. No, S.O. Kim, Vertical ZnO nanowires/graphene hybrids for transparent and flexible field emission, J. Mater. Chem. 21 (2011) 3432–3437.
[14] K.M. Wong, Y. Fang, A. Devaux, L. Wen, J. Huang, L. De Cola, Y. Lei, Assorted analytical and spectroscopic techniques for the optimization of the defect-related properties in size-controlled ZnO nanowires, Nanoscale 3 (2011) 4830–4839.
[15] Z.Z. Ye, J.Y. Huang, W.Z. Xu, J. Zhou, Z.L. Wang, Catalyst-free MOCVD growth of aligned ZnO nanotip arrays on silicon substrate with controlled tip shape, Solid State Commun. 141 (2007) 464–466.
[16] X. Zhou, T. Lin, Y. Liu, C. Wu, X. Zeng, D. Jiang, Y. Zhang, T. Guo, Structural, optical, and improved field-Emission properties of tetrapod-Shaped Sn-Doped ZnO nanostructures synthesized via thermal evaporation, Appl Mater. Interfaces 5 (2013) 10067–10073.
[17] B. Weintraub, Z. Zhou, Y. Li, Y. Deng, Solution synthesis of one-dimensional ZnO nanomaterials and their applications, Nanoscale 2 (2010) 1573–1587.
[18] Z. Fu, X. Sun, J. Zhu, B. Lin, Effect of lattice mismatch on luminescence of ZnO/Si hetero-structure, Bandaoti Xuebao 27 (2006) 239–244 (Chinese Journal of Semiconductors).
[19] F. Fang, D.X. Zhao, J.Y. Zhang, D.Z. Shen, Y.M. Lu, X.W. Fan, B.H. Li, X.H. Wang, Growth of well-aligned ZnO nanowire arrays on Si substrate, Nanotechnology 18 (2007) 235604.
[20] L. Xing, Y. Hu, P. Wang, Y. Zhao, Y. Nie, P. Deng, X. Xue, Realizing room-temperature self-powered ethanol sensing of Au/ZnO nanowire arrays

by coupling the piezotronics effect of ZnO and the catalysis of noble metal, Appl. Phys. Lett. 104 (2014) 13109.
[21] F. Fang, D.X. Zhao, J.Y. Zhang, D.Z. Shen, Y.M. Lu, X.W. Fan, B.H. Li, X.H. Wang, The influence of growth temperature on ZnO nanowires, Mater. Lett. 62 (2008) 1092–1095.
[22] J.G. Yoon, K. Kim, Growth of highly textured LiNbO3 thin film on Si with MgO buffer layer through the sol-gel process, Appl Phys. Lett. 68 (1996) 2523–2525.
[23] P. Chen, S.Y. Xie, Z.Z. Chen, Y.G. Zhou, B. Shen, R. Zhang, Y.D. Zheng, J.M. Zhu, M. Wang, X.S. Wu, Deposition and crystallization of amorphous GaN buffer layers on Si (111) substrates, J.Cryst. Growth 213 (2000) 27–32.
[24] J. Li, Z. Mei, D. Ye, H. Liang, Y. Liu, X. Du, Growth of single-crystalline Cu 2 O (111) film on ultrathin MgO modified α-Al2O3 (0001) substrate by molecular beam epitaxy, J. Cryst. Growth 353 (2012) 63–67.
[25] A. Ohtomo, M. Kawasaki, T. Koida, K. Masubuchi, H. Koinuma, Y. Sakurai, Y. Yoshida, T. Yasuda, Y. Segawa, MgxZn1-xOas a II-VI widegap semiconductor alloy, Appl Phys. Lett. 72 (1998) 2466–2468.
[26] S.J. Chen, Y.C. Liu, J.G. Ma, Y.M. Lu, J.Y. Zhang, D.Z. Shen, X.W. Fan, Effects of thermal treatment on the properties of ZnO films deposited on MgO-buffered Si substrates, J. Cryst. Growth 254 (2003) 86–91.
[27] J. Qi, J. Ren, M. Olmedo, N. Zhan, J. Liu, Unipolar resistive switching in Au/Cr/Mg0. 84Zn0. 16O2-δ/p+-Si, Appl. Phys. A 107 (2012) 891–897.
[28] S.S. Kim, B. Lee, Effects of oxygen pressure on the growth of pulsed laser deposited ZnO films on Si (001), Thin Solid Films 446 (2004) 307–312.
[29] H.Z. Zhang, X.C. Sun, R.M. Wang, D.P. Yu, Growth and formation mechanism of c-oriented ZnO nanorod arrays deposited on glass, J. Cryst. Growth 269 (2004) 464–471.
[30] J. Jeon, M. Kim, L. Jang, J.L. Hoffman, N.S. Kim, I. Lee, Effect of substrate temperature on residual stress of ZnO thin films prepared by ion beam deposition, Electron Mater. Lett. 8 (2012) 27–32.
[31] L.E. Greene, M. Law, D.H. Tan, M. Montano, J. Goldberger, G. Somorjai, P. Yang, General route to vertical ZnO nanowire arrays using textured ZnO seeds, Nano Lett. 5 (2005) 1231–1236.
[32] H. Zhang, D. Yang, X. Ma, D. Que, Synthesis and field emission characteristics of bilayered ZnO nanorod array prepared by chemical reaction, J. Phys. Chem. B 109 (2005) 17055–17059.
[33] Q. Zhao, X.Y. Xu, X.F. Song, X.Z. Zhang, D.P. Yu, C.P. Li, L. Guo, Enhanced field emission from ZnO nanorods via thermal annealing in oxygen, Appl. Phys. Lett. 88 (2006) 33102.
[34] G.G. Khan, N. Mukherjee, A. Mondal, N. Bandyopadhyay, A. Basumallick, Optical and field emission characteristics of anodic aluminium oxide/ZnO hybrid nanostructure, Mater. Chem. Phys. 122 (2010) 60–63.
[35] G. Chen, D.H. Shin, T. Iwasaki, H. Kawarada, C.J. Lee, Enhanced field emission properties of vertically aligned double-walled carbon nanotube arrays, Nanotechnology 19 (2008) 415703.
[36] J. Lu, T. Yun, M. Zheng, S.C. Haur, Enhanced field emission properties of α-Fe2O3 nanostructures with the removal of adsorbed gas molecules, J. Phys. Chem. C 115 (2011) 8816–8824.